metals

MDPI

Article

Initiation Mechanism of Localized Corrosion Induced by Al_2O_3-MnS Composite Inclusion in Low-Alloy Structural Steel

Chao Liu [1,2,*], Hao Yuan [3], Xuedong Li [1], Zhichao Che [3], Shufeng Yang [3] and Cuiwei Du [1,2]

[1] Key Laboratory for Corrosion and Protection of the Ministry of Education, Institute of Advanced Materials & Technology, University of Science and Technology Beijing, Beijing 100083, China; g20199371@xs.ustb.edu.cn (X.L.); dcw@ustb.edu.cn (C.D.)
[2] National Materials Corrosion and Protection Data Center, University of Science and Technology Beijing, Beijing 100083, China
[3] School of Metallurgical and Ecological Engineering, University of Science and Technology Beijing, Beijing 100083, China; ustbyjyuan@163.com (H.Y.); czc190909@163.com (Z.C.); yangshufeng@ustb.edu.cn (S.Y.)
* Correspondence: liuchao@ustb.edu.cn; Tel.: +86-010-62333931-502

Abstract: The present work systematically investigated the initiation mechanism of localized corrosion induced by Al_2O_3-MnS composite inclusion in E690 steel under a simulated marine environment. The results showed that a micro-gap exists between the Al_2O_3-MnS inclusion and the matrix, and electron backscattered diffraction (EBSD) analysis revealed significant lattice dislocation zones around the Al_2O_3-MnS composite inclusion. The presence of the micro-gap and the lattice dislocation both promoted the localized corrosion initiation. The Volta potential of Al_2O_3 detected by scanning Kelvin probe force microscopy (SKPFM) was approximately 149.33 mV higher than that of the steel matrix, and the Volta potential of MnS was 10 mV lower than that of the steel matrix. The current-sensing atomic force microscopy (CSAFM) results showed that the Al_2O_3 was not conductive, while the MnS had good conductive properties. Therefore, it was not possible for a galvanic couple to be formed between Al_2O_3 and the adjacent steel matrix. A galvanic couple effect between the MnS and the adjacent steel matrix was directly demonstrated for the first time. The MnS acted as the anode phase for preferential dissolution in the corrosion process. The in situ immersion experiments and the Pourbaix diagram results confirmed that the dissolution of MnS was an electrochemical reaction process and the dissolution of Al_2O_3 was a chemical reaction.

Keywords: low-alloy structural steel; composite inclusions; localized corrosion; galvanic couple corrosion

Citation: Liu, C.; Yuan, H.; Li, X.; Che, Z.; Yang, S.; Du, C. Initiation Mechanism of Localized Corrosion Induced by Al_2O_3-MnS Composite Inclusion in Low-Alloy Structural Steel. *Metals* **2022**, *12*, 587. https://doi.org/10.3390/met12040587

Academic Editor: Alberto Campagnolo

Received: 14 March 2022
Accepted: 28 March 2022
Published: 30 March 2022

1. Introduction

With the further development of marine resources, the overall performance of low-alloy steel for marine engineering has faced higher requirements [1–3]. E690 low-alloy structural steel is widely used in marine engineering equipment because of its high strength and good toughness. However, corrosion, and especially localized corrosion, becomes an important hidden factor endangering the safety of steel structures. Localized corrosion is the most serious of all forms of corrosion, and various inclusions in the steel have an important impact on the initiation of localized corrosion [4,5].

The continuity and uniformity of the steel matrix can easily be destroyed by inclusions, due to the chemical or physical property differences between the inclusions and the steel matrix. These differences are the source of localized corrosion initiated by the inclusions [6,7]. Steel smelting processes with different deoxidation methods generate different inclusions in the steel. Inclusions with different compositions diversify the localized corrosion mechanism. For example, MnS inclusions, whether in carbon-steel activation systems or stainless-steel passivation systems, are sensitive locations for pitting and stress corrosion initiation. Shinozaki et al. observed an oscillation in the anodic polarization

curve and a significant peak in the anodic current in the presence of MnS, by performing kinetic potential polarization in microregions with and without MnS [8]. It was suggested that the increase in current was mainly caused by MnS dissolution. Some other studies have suggested that there is a galvanic couple between MnS and the steel matrix, with MnS acting as the anode for preferential dissolution and the surrounding matrix acting as the cathode [7,9,10]. However, the galvanic couple assumption appears unconvincing without evidence of MnS conductivity. The addition of RE elements to steel leads to the preferential formation of rare earth oxides. Liu et al. found that the preferential dissolution of $(RE)_2O_2S$-$(RE)_xS_y$ was the main cause of localized corrosion initiation in Q460 low-alloy steel. The lower Volta potential of the rare earth oxygen sulfide resulted in its preferential dissolution [11]. Jeon et al. found that the addition of Ce to steel resulted in the formation of a stable Ce oxide, which reduced the cracking region at the matrix/inclusion interface and enhanced the pitting resistance of super duplex stainless steels [12]. Cheng et al. found that a galvanic couple was formed between TiN and the substrate, where TiN acted as the cathode, promoting the preferential dissolution of the steel matrix [13]. Xue et al. found that the (Ti, Nb)N precipitated phase with a lower Volta potential remained stable in the corrosion process, using in situ submerged AFM tracing [14].

For Al_2O_3-MnS composite inclusions, Park, I.-J et al. found that when TRIP steel was immersed in 3.5 wt.% NaCl for 30 min, MnS was preferentially dissolved to form pits, but Al_2O_3 was more stable, dissolving after 60 min of immersion [15]. Liu confirmed that the dissolution of Al_2O_3 is chemically driven and that the high degree of lattice distortion around Al_2O_3 provides the driving force for corrosion initiation [16]. Wei et al. pointed out that the galvanic effect between the MnS-Al_2O_3 inclusions resulted in the initiation of localized corrosion [10]. However, to date, the electrochemical mechanism of localized corrosion initiation induced by Al_2O_3-MnS composite inclusions has remained unclear. Without evidence of the conductivity of Al_2O_3-MnS, the possibility of a galvanic effect formed between the inclusion and the matrix seems unpersuasive.

In this study, field emission scanning electron microscopy with energy-dispersive spectrometry (FE-SEM-EDS), electron backscattered diffraction (EBSD), scanning Kelvin probe force microscopy (SKPFM), and current-sensing atomic force microscopy (CSAFM) techniques were used to reveal the mechanism of localized corrosion induced by different inclusions. The Pourbaix diagram was also adopted to analyze the thermodynamic process of the localized corrosion. Finally, the corrosion mechanism of Al_2O_3-MnS inclusions in a simulated marine solution was investigated.

2. Experiments

2.1. Materials and Methods

Aluminum deoxidized E690 steel was produced by autonomous smelting in a vacuum furnace. The steel was rolled after forging. The rolled deformation was up to 70%. The chemical composition of the steel was verified by chemical analysis. The chemical composition of the experimental steel is shown in Table 1. Specimens with a size of 10 mm × 10 mm × 3 mm were produced from the forged and rolled steel. Samples were mechanically ground to 3000 mesh with silicon carbide sandpaper and polished with 0.5 μm diamond polishing paste to eliminate the effect of surface roughness on local corrosion. Finally, the samples were ultrasonically cleaned in ethanol. To avoid the influence of the mechanical polishing process on the inclusion morphology and EBSD results, precision ion-polished samples were prepared. The specimens were manually ground to a thickness of 30 μm with silicon carbide papers and reduced with argon ions using a Gatan 691 precision ion polishing system.

Table 1. Chemical composition of the steel sample (wt.%).

C	Si	Mn	P	S	Cr	Ni	Ti	Mo	V	Nb	Al
0.047	0.214	1.277	0.008	0.011	0.54	1.222	0.031	0.54	0.035	0.051	0.108

2.2. Sample Characterization

Inclusions in the steel were initially characterized using a Zeiss Merlin FE-SEM (Zeiss, Oberkochen, Germany). The elemental distributions of the inclusions were measured using EDS (EDAX, Mahwah, NJ, USA). An accelerating voltage of 30 kV, a 10 nA probe current, and a working distance of 10 mm were used to obtain the secondary electron images and conduct the EDS analysis. The structural defects induced by non-metallic inclusions were characterized using EBSD (Genesis, Mahwah, NJ, USA).

2.3. In Situ Micro-Electrochemical Measurements

A hardness tester was used to mark the inclusions using a dot near the inclusions. The dot did not destroy the inclusions' morphological properties. The micro-electrochemical properties of different inclusions were detected using a commercial atomic force microscope (AFM, Bruker Icon, Germany) with SKPFM and CSAFM modules. Silicon tips on conductive silicon nitride cantilevers (PFQNE-AL) were employed, with a nominal resonant frequency of about 300 kHz and a nominal spring constant of about 0.8 N/m. Micro-area surface current measurements were performed using the contact mode of the Bruker Icon atomic force microscope current sensitivity detection module with a PFTUNA probe, at room temperature with a 3 V_{SCE} bias and a 0.5 Hz scan rate. More details can be found in our previous papers [11,16–18]. The morphology and chemical composition of the target inclusions were characterized by FE-SEM-EDS after the SKPFM and CSAFM test.

2.4. Immersion Test

The immersion test is an effective method for observing early localized corrosion on material surfaces. The samples with completed macrozone electrochemical measurements were immersed in the solution simulating the marine environment for 15 and 30 min. For the immersion tests, an aqueous solution (pH = 4.9) containing 0.1 wt.% NaCl, 0.05 wt.% Na_2SO_4, and 0.05 wt.% $CaCl_2$ was used to simulate the thin liquid films formed under a humid atmosphere at Xisha Island in the South China Sea. Before the examination of the corrosion morphology, a solution containing HCl and hexamethylenetetramine was used to remove the rust, and then the specimens were washed with alcohol and blow-dried with pressurized air.

3. Results

3.1. Inclusion Morphology Charaterization

The FE-SEM-EDS results showed that the main composition of the inclusions in E690 steel was Al_2O_3-MnS (as shown in Figure 1). This is a typical inclusion in aluminum deoxidized steel [19].

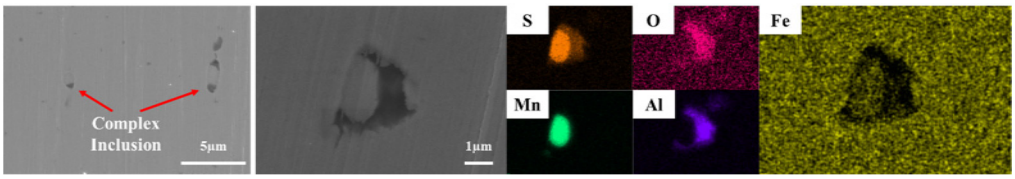

Figure 1. Morphology and composition of inclusions in specimens.

The microstructural features of the original steel may be masked by the debris produced by mechanical polishing. Thus, to avoid this negative effect, ion-polished samples were prepared. Microcracks were observed around the inclusions in the unmachined specimen (as indicated by the yellow arrows in Figure 2). Figure 2a shows an FE-SEM image of a region of Al_2O_3-MnS inclusions in the unmachined steel sample. Figure 2b shows the kernel average misorientation map (KAM map) [20]. The KAM is the average orientation error between the central pixel and its neighboring pixels. It represents the degree of local lattice distortion and gives a qualitative measure of local plastic deformation [21,22]. In the

rainbow strip in Figure 2d, blue indicates the mildly deformed areas, green areas are more deformed than blue areas, and red areas are the most deformed. The KAM diagram shows significant lattice distortion around the Al_2O_3-MnS inclusions, but the degree of distortion in the material is reduced compared to pure Al_2O_3 inclusions. This may result from the better deformability of MnS as a plastic inclusion in the forging and rolling process [23].

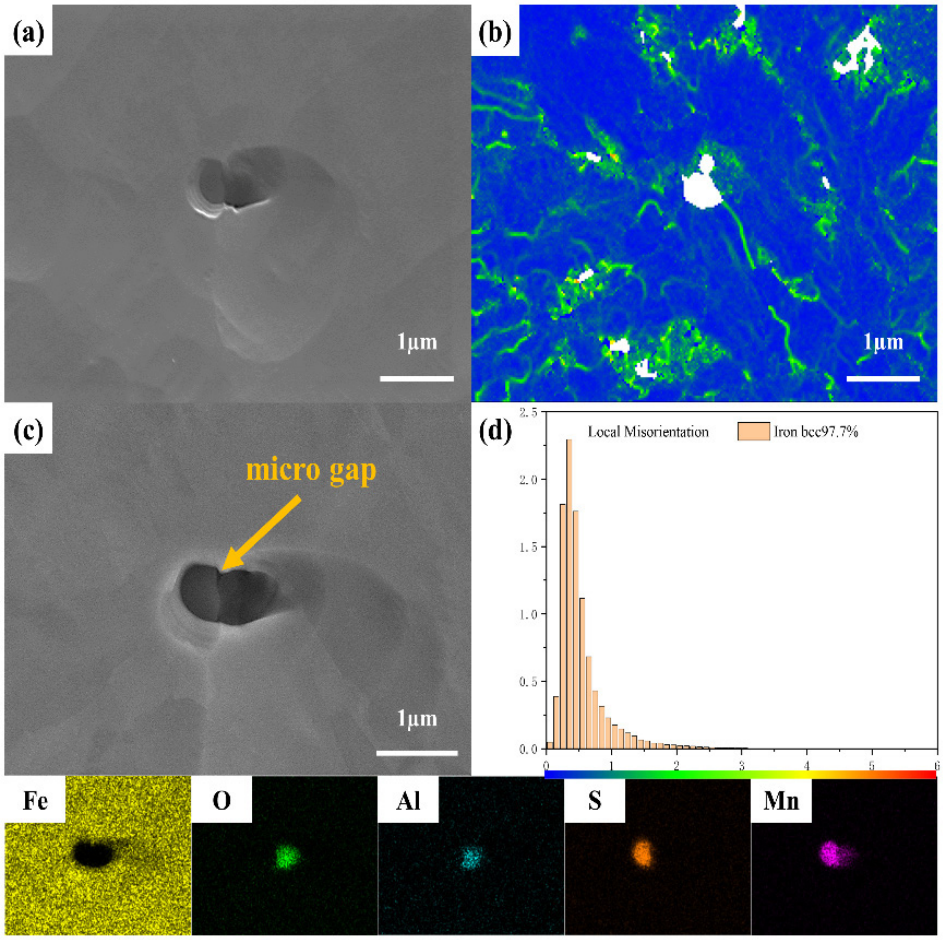

Figure 2. Analysis of Al_2O_3 inclusions and adjacent areas: (**a**) FE-SEM of EBSD; (**b**) KAM map of the same region shown in (**a**); (**c**) FE-SEM-EDS image; (**d**) the density of the local plastic deformation of inclusions.

3.2. Electrochemical Properties of Inclusions

The existence of local electrochemical inhomogeneities between the inclusions and the steel matrix is the main reason for the initiation of localized corrosion [24–26]. Therefore, SKPFM and CSAFM tests were carried out on the Al_2O_3-MnS inclusions to investigate the differences in electrochemical properties between the inclusions and the substrate. As shown in Figure 3b, it can be seen that the Al_2O_3 was slightly higher than the steel matrix and MnS. This probably mainly because Al_2O_3 has a higher hardness and maintains a higher stability during the mechanical grinding and polishing process. As shown in Figure 3c, the Volta potential of Al_2O_3 is higher than that of the steel matrix, and MnS has a lower Volta potential than the matrix. As shown in Figure 3d, the Al_2O_3 inclusion is in the central black region. This means that the electrical conductivity of Al_2O_3 is almost zero, negating the hypothesis of a galvanic couple effect formed between Al_2O_3 and the matrix. MnS showed a current of approximately 5.14 nA, indicating that it has better conductivity. This directly proves the existence of a galvanic couple effect between MnS and the steel matrix [7,27].

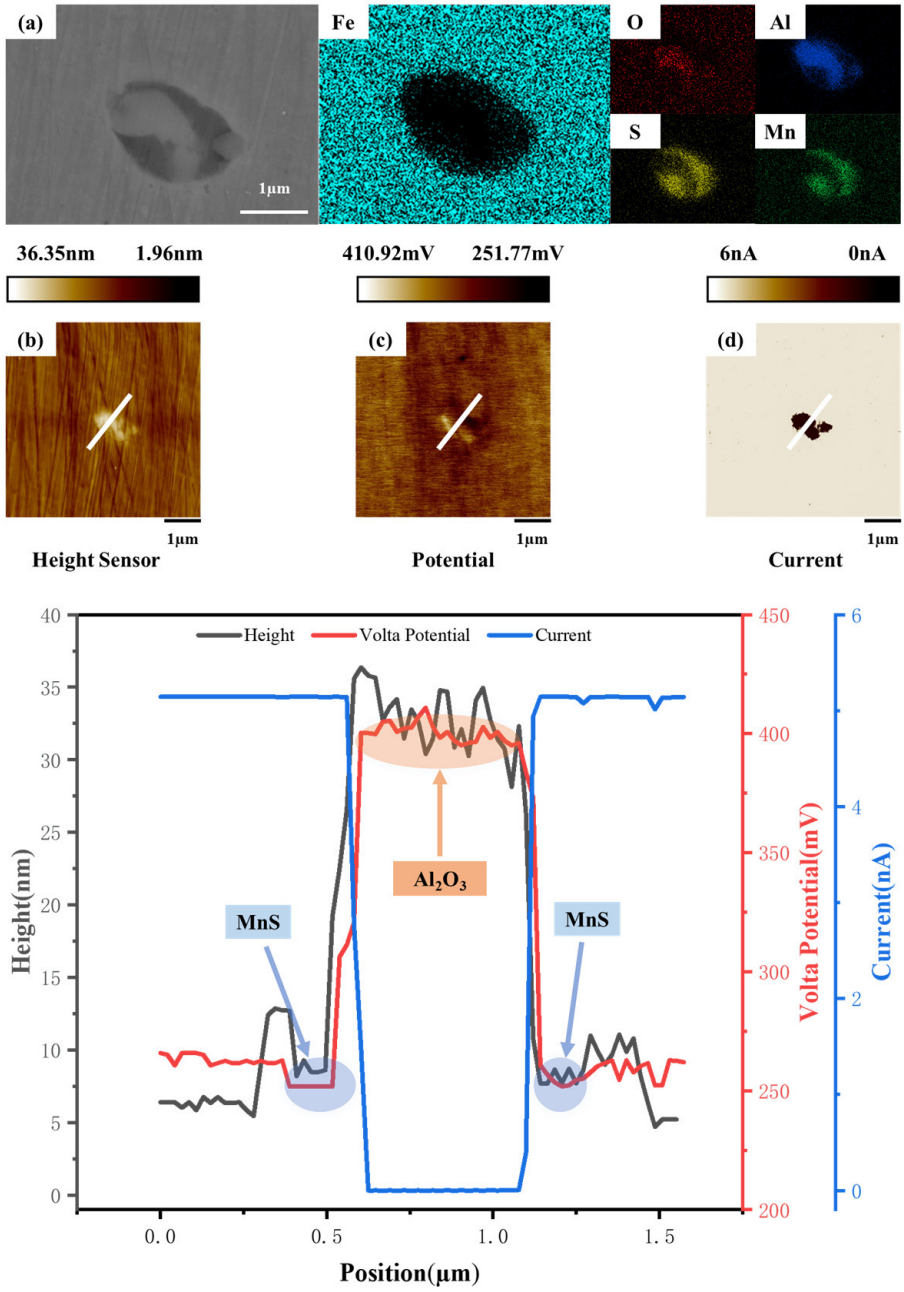

Figure 3. FE-SEM-EDS and micro-electrochemical measurements of Al_2O_3-MnS inclusions: (**a**) FE-SEM-EDS image; (**b**) AFM topography; (**c**) Volta potential; (**d**) current.

3.3. Localized Corrosion Initiation Process

The process of localized corrosion initiation caused by Al_2O_3-MnS inclusions was investigated. The corrosion process was observed by FE-SEM-EDS after immersion in a Xisha-simulating solution. The morphology and the energy spectrum of the unimpregnated Al_2O_3-MnS inclusions are shown in Figure 4a. No micro-gaps were observed between the inclusion and the steel matrix. Dissolution of the MnS inclusions was observed after 15 min immersion in the Xisha-simulating solution. The steel matrix around the inclusion was undissolved, but the distant steel matrix dissolved slightly (as shown in Figure 4b). This proves that MnS acts as an anodic phase to protect the cathodic phase (adjacent steel matrix), which agrees with the SKPFM test results. After immersion for 30 min, the residual Al_2O_3 inclusions disappeared, and deeper pits were formed. The shape of the pits is shown in Figure 4c.

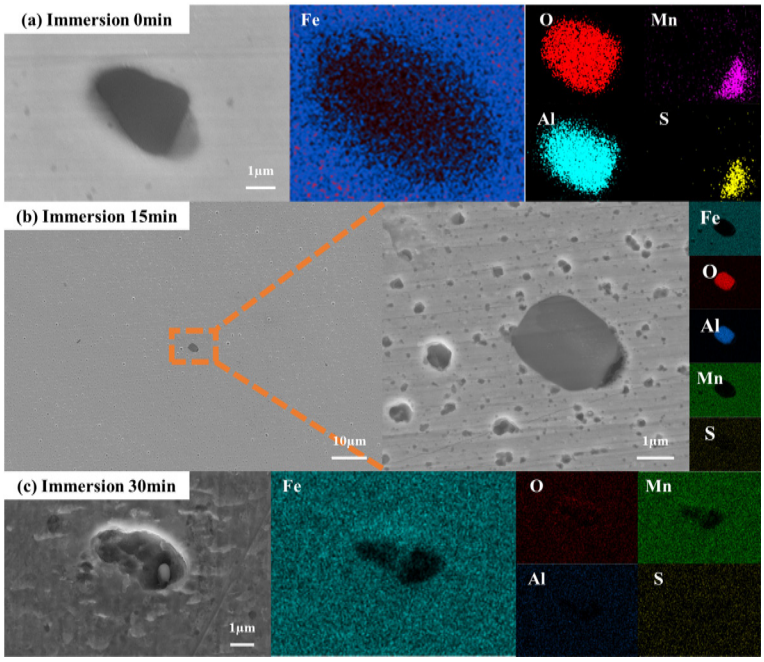

Figure 4. (**a**) The morphology and composition of inclusions in the steel, and the in situ immersion FE-SEM-EDS images of Al_2O_3-MnS inclusions after immersion (**b**) 15 min and (**c**) 30 min.

4. Discussion

In aluminum deoxidized steel, Al_2O_3-MnS is the main type of inclusion (as shown in Figure 1). Micro-gaps were found between the Al_2O_3-MnS inclusions and the steel matrix (as shown in Figure 2). They could be formed at the inclusion and the steel matrix interface, resulting from the difference in strain values [28,29] and thermal expansion coefficients between the inclusions and the steel matrix [30,31]. This provides an ideal gathering area for corrosive ions such as Cl^-.

The KAM diagram in Figure 2b shows that there is a degree of lattice distortion around the inclusions and that the corrosion resistance of the steel is highly dependent on the surface activity and dislocations of the specimen, with high-dislocation areas being prone to preferential corrosion [32–34]. The combined effect of the two can promote the appearance of localized corrosion. When the rust layer and the precipitates in the solution cover the surface of a crevice, increasing the difficulty of external oxygen transfer to the crater, the formation of an oxygen concentration difference battery accelerates the corrosion in the direction of deepening the crevice in the steel substrate [16].

The prerequisite for forming a galvanic couple is good electrical conductivity. According to the CSAFM results, Al_2O_3 exhibited insulating characteristics (Figure 3d). However, MnS had a better conductivity. Due to the lower Volta potential of MnS compared to the steel matrix (~10 mV) (Figure 3c), it is reasonable to infer that MnS, as an anodic phase, promotes the initiation of localized corrosion via the galvanic couple effect. According to the results of the immersion test (Figure 4), MnS dissolves preferentially. The matrix around the inclusions was not dissolved after 15 min of immersion, but there was slight corrosion of the distant steel matrix. This is the same type of corrosion as that identified by Li [35], demonstrating that MnS forms an electric couple with the nearby steel substrate. MnS was dissolved totally after 30 min of immersion to form pits, as shown in Figure 4c. According to the Fe-Al-H_2O Pourbaix diagram in Figure 5, the steel matrix dissolves to produce Fe^{2+} ions at pH 4.9. There is an increased Fe and Fe^{2+} content and a decreased Fe^{3+} content on the steel surface [36]. Fe^{2+} ions are hydrolyzed and form a rust layer over the pit [37–39], blocking the transport of material from the pit to the outside world. The formation of an internal and external oxygen concentration cell, where the inside of the pit is a small anode and the surrounding steel substrate is a large cathode, accelerates the corrosion of the pit in

the longitudinal direction [40]. The Al_2O_3 inclusion remains stable in the solution with a pH of 4.9. As the Cl^- concentration increases, the solution becomes more acidic under the effect of the oxygen concentration difference [41,42]. When the pH in the crater drops to the yellow region in Figure 5, Al_2O_3 cannot be stabilized and Al^{3+} is generated until it is all dissolved, forming a crater as shown in Figure 4c. As Al_2O_3 inclusions are not electrically conductive and cannot form a galvanic couple with the steel substrate, the Al_2O_3 can only be dissolved chemically, not electrochemically.

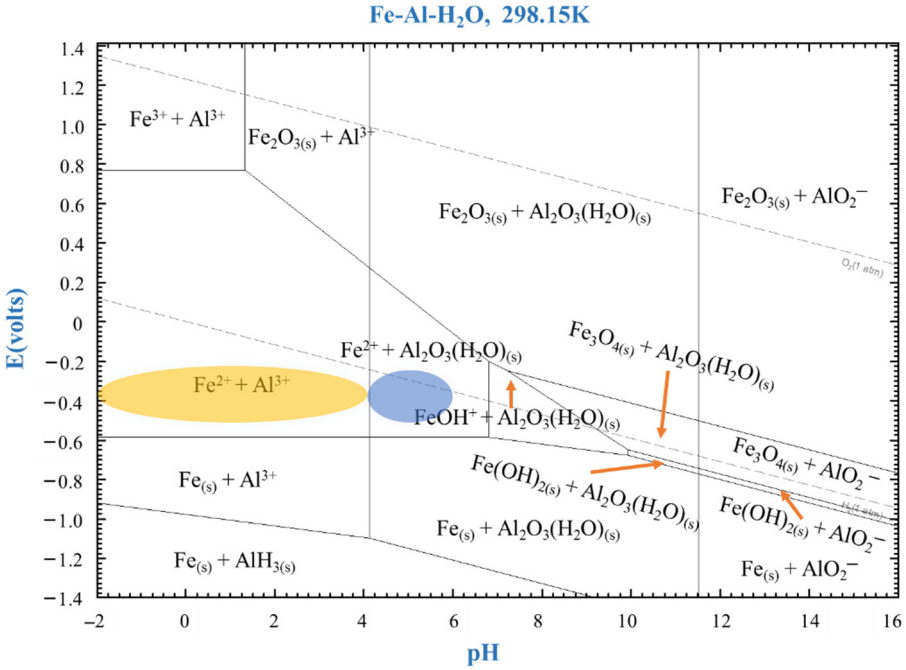

Figure 5. Pourbaix diagram of the Fe-Al-H_2O system calculated at 298.15 K using FactSage software.

A schematic diagram of the initiation and development of localized corrosion induced by Al_2O_3-MnS inclusions was drawn based on the previous analysis, as shown in Figure 6. It can be observed that:

1. With the enrichment of aggressive ions at the micro-gaps around the inclusions and the region of high activation due to lattice distortion, localized corrosion is triggered (Figure 6a).
2. A galvanic couple effect is formed between MnS and the steel substrate. Localized corrosion is promoted by the preferential dissolution of MnS as the anodic phase (Figure 6b).
3. With the MnS completely dissolved, an oxygen concentration difference battery effect is formed in the pits. This results in a sharp decrease in the solution pH in the pits (Figure 6c).
4. When the pH of the solution in the pits is lower than 4, Al_2O_3 inclusions are dissolved chemically.

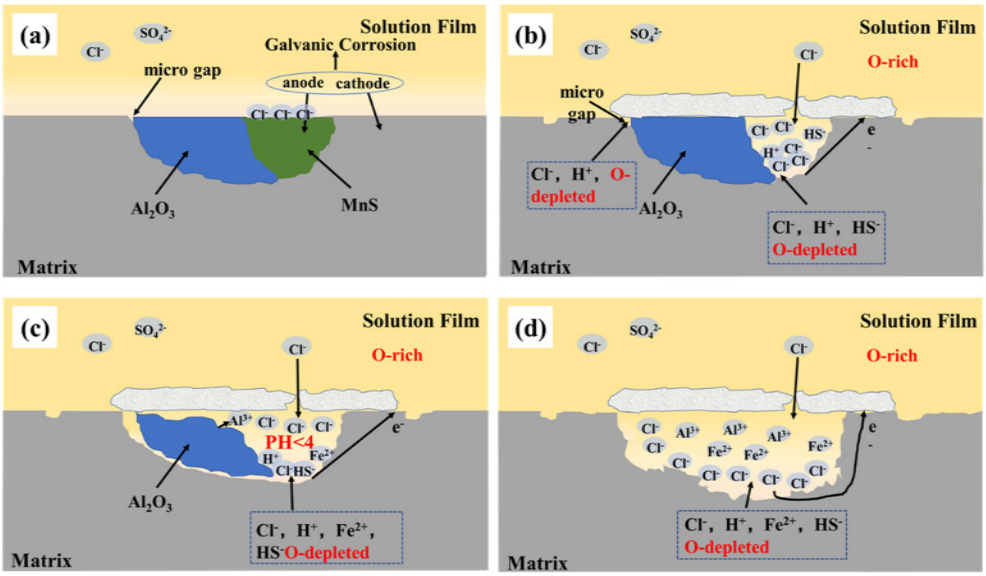

Figure 6. Schematic diagram of the process of the appearance and expansion of micro-pits caused by Al_2O_3-MnS inclusions. (**a**) Trigger of localized corrosion around inclusion, (**b**) dissolution of MnS portion, (**c**) dissolution of Al_2O_3, and (**d**) stable pits formed with inclusion dissolved.

5. Conclusions

This research analyzed the initiation mechanism of localized corrosion induced by Al_2O_3-MnS inclusions in E690 steel under a marine environment. It was found that:

1. Al_2O_3-MnS inclusions are the typical inclusions in aluminum deoxidized E690 steel. Micro-gaps and a high density of lattice dislocations could be observed around the Al_2O_3-MnS inclusions. These differences in physical properties promote the possibility of localized corrosion initiation.
2. A galvanic effect between MnS and the matrix was proved by CSAFM. MnS, with a lower Volta potential, is dissolved preferentially as the anodic phase at the corrosion initiation stage.
3. The insulating properties of Al_2O_3 confirm its inability to form a galvanic couple with the steel substrate. When the solution pH decreased in the pits after the MnS was dissolved, an oxygen concentration difference battery effect formed in the pits and the adjacent matrix. The chemical dissolution process of Al_2O_3 was also triggered in this acidic environment.
4. An initiation and evolution mechanism of localized corrosion induced by Al_2O_3-MnS complex inclusion was established.

Author Contributions: C.L.: conceptualization, writing—original draft, writing—review and editing; H.Y.: methodology, investigation, writing—original draft; X.L.: investigation; Z.C.: methodology; S.Y.: project administration, supervision; C.D.: project administration, supervision. All authors have read and agreed to the published version of the manuscript.

Funding: This research was funded by the National Nature Science Foundation of China, under grant number 52104319 and by the National Science and Technology Resources Investigation Program of China (Grant No. 2019FY101400).

Data Availability Statement: Not applicable.

Acknowledgments: The authors would like to thank Yilun Li and Zaihao Jiang at the University of Science and Technology Beijing, for assistance with the calculations.

Conflicts of Interest: The authors declare that they have no known competing financial interests or personal relationships that could have appeared to influence the work reported in this paper.

References

1. Ali, L.; Khan, S.; Bashmal, S.; Iqbal, N.; Dai, W.; Bai, Y. Fatigue crack monitoring of T-type joints in steel offshore oil and gas jacket platform. *Sensors* **2021**, *21*, 3294. [CrossRef] [PubMed]
2. Rui, Z.; Li, C.; Peng, F.; Ling, K.; Chen, G.; Zhou, X.; Chang, H. Development of industry performance metrics for offshore oil and gas project. *J. Nat. Gas Sci. Eng.* **2017**, *39*, 44–53. [CrossRef]
3. Zhou, Y.; Engelberg, D.L. On the application of bipolar electrochemistry to characterise the localised corrosion behaviour of type 420 ferritic stainless steel. *Metals* **2020**, *10*, 794. [CrossRef]
4. Cao, Y.; Li, G.; Hou, Y.; Moelans, N.; Guo, M. DFT study on the mechanism of inclusion-induced initial pitting corrosion of Al-Ti-Ca complex deoxidized steel with Ce treatment. *Phys. B Condens. Matter* **2019**, *558*, 10–19. [CrossRef]
5. Zheng, S.; Li, C.; Qi, Y.; Chen, L.; Chen, C. Mechanism of (Mg, Al, Ca)-oxide inclusion-induced pitting corrosion in 316L stainless steel exposed to sulphur environments containing chloride ion. *Corros. Sci.* **2013**, *67*, 20–31. [CrossRef]
6. Avci, R.; Davis, B.H.; Wolfenden, M.L.; Beech, I.B.; Lucas, K.; Paul, D. Mechanism of MnS-mediated pit initiation and propagation in carbon steel in an anaerobic sulfidogenic media. *Corros. Sci.* **2013**, *76*, 267–274. [CrossRef]
7. Vuillemin, B.; Philippe, X.; Oltra, R.; Vignal, V.; Coudreuse, L.; Dufour, L.C.; Finot, E. SVET, AFM and AES study of pitting corrosion initiated on MnS inclusions by microinjection. *Corros. Sci.* **2003**, *45*, 1143–1159. [CrossRef]
8. Shinozaki, J.; Muto, I.; Omura, T.; Numata, M.; Hara, N. Local dissolution of MnS inclusion and microstructural distribution of absorbed hydrogen in carbon steel. *J. Electrochem. Soc.* **2011**, *158*, C302–C309. [CrossRef]
9. Qiu, J.; Leng, B.; Liu, H.; Macdonald, D.D.; Wu, A.; Jia, Y.; Zhou, X. Effect of SO_4^{2-} on the corrosion of 316L stainless steel in molten FLiNaK salt. *Corros. Sci.* **2018**, *144*, 224–229. [CrossRef]
10. Wei, J.; Dong, J.H.; Ke, W.; He, X.Y. Influence of inclusions on early corrosion development of ultra-low carbon bainitic steel in NaCl solution. *Corrosion* **2015**, *71*, 1467–1480. [CrossRef]
11. Liu, C.; Jiang, Z.; Zhao, J.; Cheng, X.; Liu, Z.; Zhang, D.; Li, X. Influence of rare earth metals on mechanisms of localised corrosion induced by inclusions in Zr-Ti deoxidised low alloy steel. *Corros. Sci.* **2020**, *166*, 108463. [CrossRef]
12. Jeon, S.H.; Kim, S.T.; Choi, M.S.; Kim, J.S.; Kim, K.T.; Park, Y.S. Effects of cerium on the compositional variations in and around inclusions and the initiation and propagation of pitting corrosion in hyperduplex stainless steels. *Corros. Sci.* **2013**, *75*, 367–375. [CrossRef]
13. Chen, H.; Lu, L.; Huang, Y.; Li, X. Insight into TiN inclusion induced pit corrosion of interstitial free steel exposed to aerated NaCl solution. *J. Mater. Res. Technol.* **2021**, *13*, 13–24. [CrossRef]
14. Xue, W.; Li, Z.; Xiao, K.; Yu, W.; Song, J.; Chen, J.; Li, X. Initial microzonal corrosion mechanism of inclusions associated with the precipitated (Ti, Nb) N phase of Sb-containing weathering steel. *Corros. Sci.* **2020**, *163*, 108232. [CrossRef]
15. Park, I.J.; Lee, S.M.; Kang, M.; Lee, S.; Lee, Y.K. Pitting corrosion behavior in advanced high strength steels. *J. Alloys Compd.* **2015**, *619*, 205–210. [CrossRef]
16. Liu, C.; Revilla, R.I.; Zhang, D.; Liu, Z.; Lutz, A.; Zhang, F.; Terryn, H. Role of Al_2O_3 inclusions on the localized corrosion of Q460NH weathering steel in marine environment. *Corros. Sci.* **2018**, *138*, 96–104. [CrossRef]
17. Liu, C.; Li, X.; Revilla, R.I.; Sun, T.; Zhao, J.; Yang, S.; Li, X. Towards a better understanding of localised corrosion induced by typical non-metallic inclusions in low-alloy steels. *Corros. Sci.* **2021**, *179*, 109150. [CrossRef]
18. Liu, C.; Revilla, R.I.; Liu, Z.; Zhang, D.; Li, X.; Terryn, H. Effect of inclusions modified by rare earth elements (Ce, La) on localized marine corrosion in Q460NH weathering steel. *Corros. Sci.* **2017**, *129*, 82–90. [CrossRef]
19. Zhao, D.; Li, H.; Gao, P.; Yang, J.; Hao, L. Inclusion formation and deformation in Al-killed wheel steel without calcium treatment. *Iron* **2016**, *51*, 25–32.
20. Iyer, A.H.; Stiller, K.; Leijon, G.; Andersson-Östling, H.C.; Colliander, M.H. Influence of dwell time on fatigue crack propagation in Alloy 718 laser welds. *Mater. Sci. Eng. A* **2017**, *704*, 440–447. [CrossRef]
21. Tofique, M.W.; Bergström, J.; Svensson, K.; Johansson, S.; Peng, R.L. ECCI/EBSD and TEM analysis of plastic fatigue damage accumulation responsible for fatigue crack initiation and propagation in VHCF of duplex stainless steels. *Int. J. Fatigue* **2017**, *100*, 251–262. [CrossRef]
22. Wickström, L.; Mingard, K.; Hinds, G.; Turnbull, A. Microcrack clustering in stress corrosion cracking of 22Cr and 25Cr duplex stainless steels. *Corros. Sci.* **2016**, *109*, 86–93. [CrossRef]
23. Huang, F.-Y.; Su, Y.-H.F.; Kuo, J.-C. High-temperature deformation behavior of MnS in 1215MS steel. *Met. Mater. Int.* **2018**, *24*, 1333–1345. [CrossRef]
24. Jorcin, J.B.; Orazem, M.E.; Pébère, N.; Tribollet, B. CPE analysis by local electrochemical impedance spectroscopy. *Electrochim. Acta* **2006**, *51*, 1473–1479. [CrossRef]
25. Tan, Y. Understanding the effects of electrode inhomogeneity and electrochemical heterogeneity on pitting corrosion initiation on bare electrode surfaces. *Corros. Sci.* **2011**, *53*, 1845–1864. [CrossRef]
26. Zhang, D.-L.; Wang, W.; Li, Y. An electrode array study of electrochemical inhomogeneity of zinc in zinc/steel couple during galvanic corrosion. *Corros. Sci.* **2010**, *52*, 1277–1284. [CrossRef]
27. Krawiec, H.; Vignal, V.; Oltra, R. Use of the electrochemical microcell technique and the SVET for monitoring pitting corrosion at MnS inclusions. *Electrochem. Commun.* **2004**, *6*, 655–660. [CrossRef]
28. Wranglén, G. Review article on the influence of sulphide inclusions on the corrodibility of Fe and steel. *Corros. Sci.* **1969**, *9*, 585–602. [CrossRef]

29. Yu, H.L.; Liu, X.H.; Bi, H.Y.; Chen, L.Q. Deformation behavior of inclusions in stainless steel strips during multi-pass cold rolling. *J. Mater. Process. Technol.* **2009**, *209*, 455–461. [CrossRef]
30. Song, G.; Atrens, A.; Stjohn, D.; Nairn, J.; Li, Y. The electrochemical corrosion of pure magnesium in 1 N NaCl. *Corros. Sci.* **1997**, *39*, 855–875. [CrossRef]
31. Vignal, V.; Oltra, R.; Josse, C. Local analysis of the mechanical behaviour of inclusions-containing stainless steels under straining conditions. *Scr. Mater.* **2003**, *49*, 779–784. [CrossRef]
32. Wang, C.; Yu, Y.; Yu, J.; Zhang, Y.; Wang, F.; Li, H. Effect of the macro-segregation on corrosion behavior of CrMnFeCoNi coating prepared by arc cladding. *J. Alloys Compd.* **2020**, *846*, 156263. [CrossRef]
33. Zhang, X.; Zhou, X.; Nilsson, J.O.; Dong, Z.; Cai, C. Corrosion behaviour of AA6082 Al-Mg-Si alloy extrusion: Recrystallized and non-recrystallized structures. *Corros. Sci.* **2018**, *144*, 163–171. [CrossRef]
34. Zhang, X.X.; Zhou, X.R.; Hashimoto, T.; Lindsay, J.; Ciuca, O.; Luo, C.; Tang, Z. The influence of grain structure on the corrosion behaviour of 2A97-T3 Al-Cu-Li alloy. *Corros. Sci.* **2017**, *116*, 14–21. [CrossRef]
35. Li, G.; Wang, L.; Wu, H.; Liu, C.; Wang, X.; Cui, Z. Dissolution kinetics of the sulfide-oxide complex inclusion and resulting localized corrosion mechanism of X70 steel in deaerated acidic environment. *Corros. Sci.* **2020**, *174*, 108815. [CrossRef]
36. Zhu, Y.F.; Du, R.G.; Chen, W.; Hu, R.G.; Shi, H.Y.; Guo, Y.; Lin, C.J. Study on the Corrosion Behavior of Reinforcing Steel by Electrochemical Techniques and XPS. *ECS Trans.* **2012**, *41*, 71–79. [CrossRef]
37. Tachibana, S.; Cai, B.; Davenport, A.J.; Miura, S.; Wang, H.; Dolbnya, I.P. Influence of microdefects in rust layer of weathering steel on corrosion resistance from 3D observation by synchrotron X-ray micro tomography. *Mater. Today Commun.* **2022**, *31*, 103219. [CrossRef]
38. Wang, Y.; Li, J.; Wang, Q.; Wang, T. Some new discoveries on the structure of the rust layer of weathering steel in a simulated industrial atmosphere by STEM-EDS and HRTEM. *Corros. Sci.* **2021**, *183*, 109322. [CrossRef]
39. Wu, F.; Hu, Z.; Liu, X.; Su, C.; Hao, L. Understanding in compositional phases of carbon steel rust layer with a long-term atmospheric exposure. *Mater. Lett.* **2022**, *315*, 131968. [CrossRef]
40. Wranglen, G. Pitting and sulphide inclusions in steel. *Corros. Sci.* **1974**, *14*, 331–349. [CrossRef]
41. Guo, Y.; Wang, X.; Zhu, Y.; Zhang, J.; Gao, Y.; Yang, Z.; Lin, C.J. Electrochemical and XPS study on effect of Cl-on corrosion behavior of reinforcing steel in simulated concrete pore solutions. *Int. J. Electrochem. Sci.* **2013**, *8*, 12769.
42. Jiang, X.; Nešić, S.; Kinsella, B.; Brown, B.; Young, D. Electrochemical investigation of the role of Cl− on localized carbon dioxide corrosion behavior of mild steel. *Corrosion* **2013**, *69*, 15–24. [CrossRef]